CFD SIMULATION AND OPTIMIZATION OF HEAT TRANSFER ENHANCEMENT IN HEV STATIC MIXERS WITH ROTATED ANGLES FOR TURBULENT FLOWS

by

Noureddine KAID[a], Ali AKGUL[b,c*], Mohammed Ayad ALKHAFAJI[d], Karrar S. MOHSEN[e], Jihad ASAD[f], Rabab JARRAR[f], Hussein SHANAK[f], Younes MENNI[a], and Sherzod ABDULLAEV[g,h]

[a] Department of Technology, University Center Salhi Ahmed Naama (Ctr. Univ. Naama), Naama, Algeria
[b] Department of Mathematics, Art and Science Faculty, Siirt University, Siirt, Turkey
[c] Department of Electronics and Communication Engineering, Saveetha School of Engineering, SIMATS, Chennai, Tamilnadu, India
[d] College of Engineering, National University of Science and Technology, Dhi Qar, Iraq
[e] Information and Communication Technology Research Group, Scientific Research Center, Al-Ayen University, Thi-Qar, Iraq
[f] Department of Physics, Faculty of Applied Science, Palestine Technical University-Kadoorie, Tulkarm, Palestine
[g] Faculty of Chemical Engineering, New Uzbekistan University, Tashkent, Uzbekistan
[h] Department of Science and Innovation, Tashkent State Pedagogical University named after Nizami, Tashkent, Uzbekistan

Original scientific paper
https://doi.org/10.2298/TSCI2304123K

Static mixers are becoming increasingly popular because they are energy-efficient, cost-effective, and easy to maintain. Mixing is an essential unit operation in many chemical industries. In this study, a modified high efficiency vortex static mixer was used to examine laminar flows in a rectangular duct. To encourage fluid rotation and improve mixing with heat transfer, the modified high efficiency vortex set was rotated by angles of 0°, 5°, 10°, 20°, 25°, and 30°. The Reynolds number varied from 3000 to 8000. The outcomes demonstrated that the performance of the mixing was significantly impacted by the modified high efficiency vortex set. The highest mixing efficiency was achieved with a rotation angle between 15° and 20°. Furthermore, the rotations reduced pressure loss in the system and enhanced heat transfer performance, by creating vortices. These results show how modified high efficiency vortex static mixers can improve mixing and heat transfer efficiency in turbulent flows, with prospective utilization across diverse chemical sectors.

Key words: *static mixers, chemical industries, modified high efficiency vortex, rectangular duct, mixing efficiency.*

Introduction

Mixing is an essential unit operation found in nearly all chemical industries [1]. Static mixers, also known as motionless mixers, have gained wide acceptance due to their ad-

* Corresponding author, e-mail: aliakgul00727@gmail.com

vantages such as low power consumption, low capital investment, minimal maintenance requirements, and high versatility [2, 3]. They operate without any moving parts and have demonstrated superior performance compared to traditional dynamic mixers, including improved blending efficiency, reduced pressure drop, and higher throughput [4-7]. The high efficiency vortex (HEV) mixer distinguishes itself among other static mixers due to its superior capability in turbulent blending of gases or miscible liquids [8-10]. Conversely, helical mixing elements find frequent application in in-line blending scenarios characterized by laminar and transitional flow conditions [2, 11-13]. The HEV mixer exhibits the generation of coherent structures, manifested as longitudinal counter-rotating vortices, which effectively promote radial mass transfer, particle dispersion, and mixing. It has been used in the process industries for liquid-liquid and gas-gas mixing, offering a wide range of applications and scales [10]. The HEV mixer has significantly lower energy costs, making it a desirable choice for applications such as emulsification. The mixer's ability to generate streamwise vortices and shear-instability-driven flow structures behind the vortex generators has been found to play a crucial role in convective transport phenomena, enhancing heat and mass transfer processes [9, 14]. Experimental findings of [15] revealed that the mixer induces a complex vortex system, comprising a persistent longitudinal vortex and temporary hairpin vortices. The computational model accurately predicted the presence of the longitudinal vortex and observed a notable turbulence intensity in the hairpin vortex region. In a study conducted by [16], a novel HEV static mixer was employed to augment the heat transfer coefficient of a drag-reducing fluid, Ethoquad, in combination with sodium salicylate. Remarkable enhancements in heat transfer coefficients were observed, with Nusselt numbers exhibiting three to fivefold increases compared to conventional flow conditions without the presence of a mixer. The computational and experimental analysis demonstrates a strong agreement between predicted and measured data for the fined tape insert. The findings suggest that the vortex flow induced by the insert promotes impingement/reattachment flows along the duct walls [17, 18], resulting in a significant enhancement in heat transfer rate. These observations were made by Pongjet Promvonge. Simulation studies were conducted to investigate the impact of different apical angles and the number of triangles on the mixing effect [19]. The results demonstrated that an increase in the apical angle of the triangles, ranging from 30° to 150°, led to an improvement in the mixing effect. Moreover, experimental, and numerical investigations have been conducted to analyze the effects of hydrodynamics on transfer processes in the HEV static mixer. These studies have demonstrated the high energy efficiency of the HEV mixer in turbulent flows with embedded vorticity [20-23].

This study aims to investigate the impact of the modified high-efficiency vortex (MHEV) with the objective of mitigating pressure loss, enhancing mixing efficiency, and improving heat transfer characteristics. The study seeks to elucidate the potential benefits of this approach in optimizing the performance of the HEV for various industrial applications.

Presentation of the case study:
Numerical simulation and geometry

The study focuses on investigating the effects of a rotational geometrical configuration on the performance of a HEV static mixer within a rectangular tube. The geometry of the problem consists of a rectangular tube with an inlet side length, *D*, of 50 mm and a length of 20 times *D*. The HEV is characterized by varying rotational angles (rot = 0°, 5°, 10°, 15°, 20°, 25°, and 30°). To achieve fully developed flow at the inlet and prevent the occurrence of reversed flows at the outlet, extended regions were introduced at both the inlet and outlet sec-

tions of the duct. This approach was adopted to ensure the desired flow characteristics and maintain the integrity of the flow field throughout the system. The working fluid employed in the study is air, see figs. 1-3 for the visualization of the geometry.

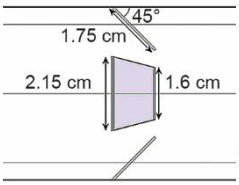

Figure 1. The HEV dimensions

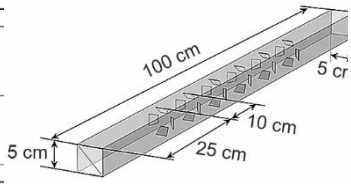

Figure 2. Rectangular duct sizing

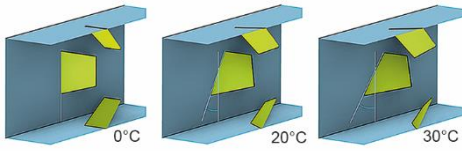

Figure 3. Rotational modifications on the HEV

Boundary conditions

The study involved determining velocity and temperature profiles at the inlet section of a rectangular duct. At the inlet boundary, a uniform air velocity, U_{in}, was determined based on the Reynolds number, while a constant inlet temperature, T_{in} = 27 °C, was prescribed. The entrance of air was divided diagonally, with each section having a specie concentration, $C_0 = 0$ and $C_1 = 1$ mol/m^3, fig. 4. The exit boundary condition was set as atmospheric pressure. Throughout the system, the physical properties of air, including density and viscosity, were assumed to be constant. The rectangular duct walls and the MHEV elements were treated with a no-slip wall condition.

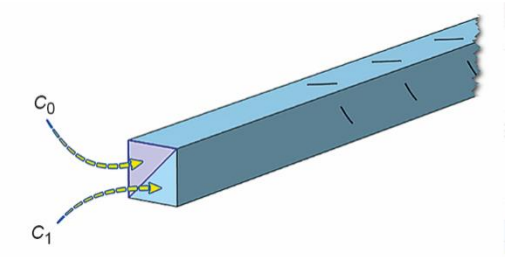

Figure 4. Inlet species concentration

The walls of the duct were maintained at a constant temperature T_w = 77 °C, while the MHEV were considered adiabatic walls with no heat transfer between them and the fluid. The study encompassed a range of Reynolds numbers, varying from 3000 to 8000.

Governing equations

Among various turbulence models, the standard k-ε turbulence model stands out for its reliability, robustness, and faster convergence rate compared to other models. It provides accurate predictions for turbulent flow and heat transfer phenomena.

The flow within the duct is described by the RANS equations and the energy equation, which govern the behavior of incompressible turbulent flows. These equations can be formulated as follows.

Continuity equation:

$$\frac{\partial}{\partial x_i}(\rho u_i) = 0 \tag{1}$$

The principle of momentum conservation can be defined:

$$\frac{\partial}{\partial x_i}(\rho u_i u_j) = \frac{\partial}{\partial x_i}\left[\mu\left(\frac{\partial u_i}{\partial u_j} - \overline{\rho u_i' \rho u_j'}\right)\right] - \frac{\partial p}{\partial x_i} \tag{2}$$

Additionally, the equation governing energy conservation is:

$$\frac{\partial}{\partial x_i}(\rho u_i T) = \frac{\partial}{\partial x_i}\left(\frac{k}{C_p}\frac{\partial T}{\partial x_j}\right) \tag{3}$$

In this study, the *k-ε* standard model of turbulence is employed, which relies on the representation of turbulent kinetic energy, *k*, and energy dissipation, *ε*, as described by eqs. (6) and (7), respectively.

$$\frac{\partial}{\partial x_i}(\rho k u_i) = \frac{\partial}{\partial x_j}\left[\left(\mu + \frac{\mu_T}{\sigma_k}\right)\frac{\partial k}{\partial x_j}\right] + P_k - \rho_\varepsilon \tag{6}$$

$$\frac{\partial}{\partial x_i}(\rho \varepsilon u_i) = \frac{\partial}{\partial x_j}\left[\left(\mu + \frac{\mu_T}{\sigma_\varepsilon}\right)\frac{\partial \varepsilon}{\partial x_j}\right] + C_{1\varepsilon}\frac{\varepsilon}{k}P_k - C_{2\varepsilon}\rho\frac{\varepsilon^2}{k} \tag{7}$$

where $\mu_T = \rho C_\mu (k^2/\varepsilon)$, $P_\mathrm{k} = \mu_T\{\nabla\mathbf{u}:[\nabla\mathbf{u} + (\nabla\mathbf{u})^T]\}$, μ_T is the turbulent viscosity and P_k – the turbulent kinetic energy generated by the mean velocity gradients.

In the present simulation, the model constants are represented as $C_{1\varepsilon}$, $C_{2\varepsilon}$, C_μ, σ_k and σ_ε:

$$C_{1\varepsilon} = 1.44, \quad C_{2\varepsilon} = 1.92, \quad C_\mu = 0.09, \sigma_k = 1.0, \quad \sigma_\varepsilon = 1.3$$

Heat transfer enhancement is evaluated by calculating the local and averaged Nusselt number and friction factor, *f*, according to the following equations:

$$\mathrm{Nu} = \frac{hL}{k} \tag{8}$$

Averaged Nusselt number:

$$\overline{\mathrm{Nu}} = \frac{\frac{1}{L}\int_0^L h_x \mathrm{d}xL}{k} = \frac{\bar{h}L}{k} \tag{9}$$

Darcy friction factor:

$$f = \frac{2}{\frac{L}{D_h}}\frac{\Delta P}{\rho {U_0}^2} \tag{10}$$

Static mixers are evaluated based on their performance using the coefficient of variation (CoV), which measures the intensity of segregation. The CoV is the ratio of the standard deviation, *σ*, to the mean concentration, *C*, of the species, as shown in eq. (11). A CoV below 0.05 is typically considered sufficient for mixing, but for unmixed fluids, the CoV tends to approach 1:

$$CoV = \frac{\sqrt{\frac{1}{N}\sum_i^N \left(C_i - \bar{C}\right)^2}}{\bar{C}} \tag{11}$$

where C_i is the punctual concentration of pixels, $\bar{C}$ – the average concentration, and N – the number of points sampled.

The mixing index (MI) evaluates how quickly a combination reaches equilibrium. This is a sign of how well the mixing process was done:

$$MI = 1 - CoV \tag{12}$$

Computational approach

The geometric configuration of the system under investigation was created and discretized using a tetrahedral mesh element, as depicted in fig. 5. The choice of mesh type is crucial in achieving accurate results, and tetrahedral meshes are particularly advantageous for handling complex geometries. To optimize the mesh density, a series of mesh tests were conducted for the smooth duct (without HEV), ranging from 302590 to 3295585 mesh elements. The precision of the results was observed to stabilize at 1014688 elements, with average outlet temperature variations within 3.2% to 1.8% as the mesh density increased further, for Reynolds number in the range of 3000 to 8000. A similar approach was adopted for other geometric configurations with HEV, adjusting the grid element count between 1536709 and 1737194 elements.

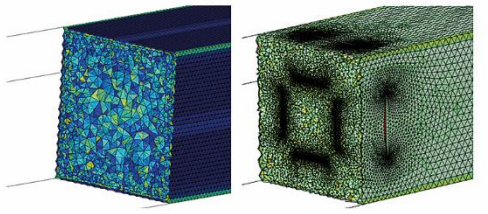

Figure 5. Generated grid with tetrahedral mesh

The flow regime within the tube is characterized as turbulent, and the dynamics of the flow are described by the RANS equation, supplemented by the standard *k-ε* turbulence model and the energy equation. The chosen turbulence model effectively captures the turbulent characteristics of the flow, while the energy equation accounts for the transport of thermal energy. The conducted investigations have demonstrated stability in the flow regime, confirming the persistence of turbulent behavior throughout the examined system.

The computational simulations achieved convergence within approximately 17 hours for all parameters. The numerical computations were performed on a desktop computer featuring a Ryzen 9 3900X 12-Core Processor, 64 Gigabytes of Memory, and a processing speed of 3.80 Gigahertz. The used operating system was a 64-bit Windows 10 Pro, Version 21H2, with OS build 19044.2130.

Validation, outcomes, and discussions

The predicted results on frictional characteristics in a smooth rectangular duct are validated by verifying the values of the friction factor, *f*. Under identical geometric and operating conditions, our findings are compared to those obtained using the correlations of Blasius, Gnielinski, and Petukhov for the friction factor, tab. 1.

Table 1. Friction factor correlations

Correlation	Equation
Balsius (1913)	$f = 0.3164 \times \mathrm{Re}^{-0.25}$ for $\mathrm{Re} \leq 2.10^4$
Petukhov (1970)	$f = (1.82 \times \log\mathrm{Re} - 1.64)^{-2}$ for $3000 < \mathrm{Re} < 5.10^6$
Gnielinski (1976)	$f = (0.76 \times \ln\mathrm{Re} - 1.64)^{-2}$ for $2300 \leq \mathrm{Re} \leq 5.10^6$

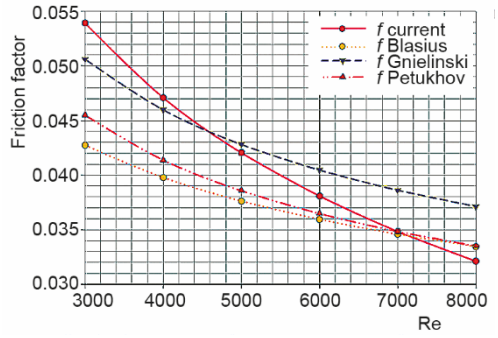

Figure 6. Validation of friction with various correlations

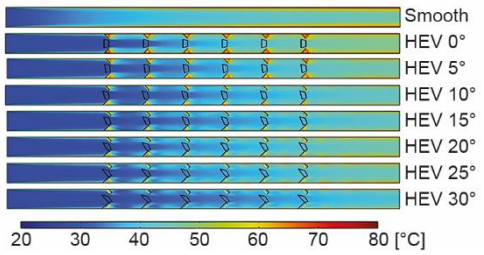

Figure 7. Surface temperature along the channel for various geometries, Re = 6000

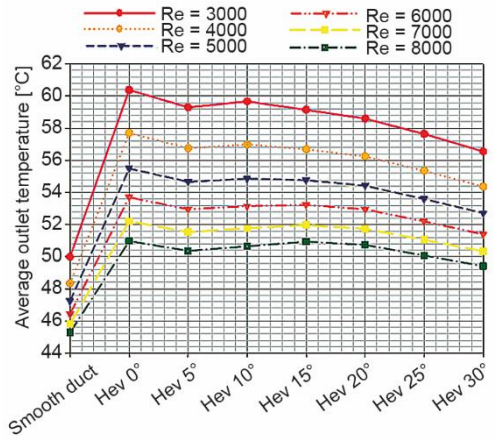

Figure 8. Avgerage output temperature *vs.* different geometries

The comparison between the friction factor, *f*, and Reynolds number graphs in fig. 6 reveals a remarkable concordance between the results obtained from the current simulation and those derived from different correlations. The plotted data points for each correlation closely align with the corresponding trendline, indicating a consistent agreement in the predicted friction factor values across the range of Reynolds numbers examined. This observation reinforces the reliability and accuracy of the simulation results, validating their conformity with established correlations commonly employed in the field.

The examination of figs. 7 and 8 provides valuable insights into the heat exchange characteristics of the rectangular duct. It is observed that significant variations in temperature occur along the walls of the duct, particularly in the vicinity behind the HEV where recirculation zones are present.

In contrast, the temperature gradient is relatively weak for the rotated HEV configurations. Moreover, the implementation of the HEV results in an enhancement in heat transfer ranging from 14% to 20% compared to a smooth duct.

However, it should be noted that this enhancement diminishes as the Reynolds number increases. These findings emphasize the influence of the HEV on heat transfer performance in the rectangular duct, highlighting the potential benefits of utilizing such a design for heat exchange applications.

The results obtained from the concentration data analysis provide valuable insights regarding the performance of a rotated HEV, see fig. 9. These findings differ from those related to heat transfer and focus on the mixing characteristics and pressure drop within the system. Initially, in a smooth duct without rotation, the mixing index is found to be poor. This indicates limited intermingling of fluid streams and suggests a lower level of mixing efficiency. However, when the HEV is introduced without rotation, an acceptable improvement in the mixing index is observed. Although the mixing performance improves, there is a higher-pressure drop associated with this configuration. Interestingly, as the rotation of the HEV is introduced, there is a notable enhancement in the mix-

ing index. This suggests that the rotational movement of the HEV promotes the mixing of fluid streams, leading to a more homogeneous mixture. Simultaneously, there is a decrease in pressure drop, indicating a reduction in energy losses within the system.

Remarkably, the most valuable results in terms of the mixing index are observed within a rotation range of 15° to 20°. Within this range, an optimal balance is achieved, where the mixing efficiency is significantly improved while maintaining an acceptable level of pressure loss, as seen in figs. 10 and 11. These findings highlight the importance of considering both mixing performance and pressure drop when analyzing the performance of a rotated HEV. The results demonstrate that proper rotation of the HEV can effectively enhance the mixing index while minimizing the associated pressure loss, ultimately leading to improved system performance in practical applications.

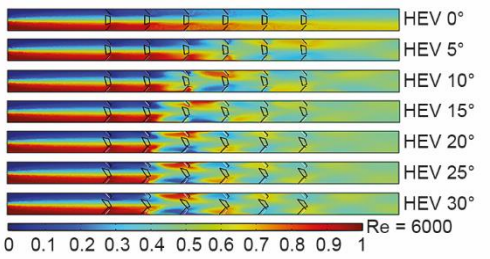

Figure 9. Concentration distribution for various geometries, Re = 6000

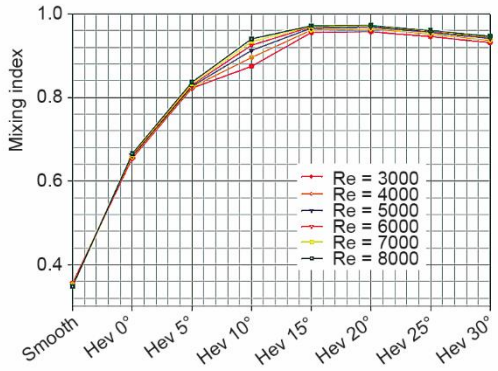

Figure 10. Mixing index for different geometries

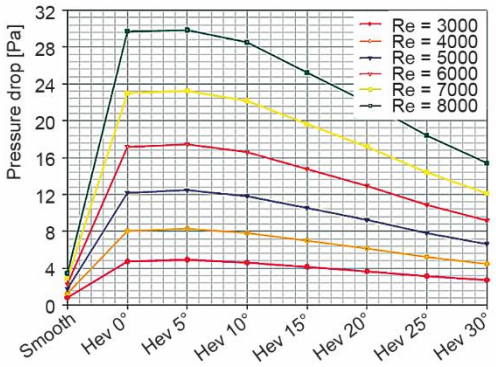

Figure 11. Pressure drop for different geometries

The average Nusselt number is calculated for various duct geometries to evaluate heat transfer characteristics. The analysis reveals that the highest Nusselt numbers are observed at 0° HEV rotation and 15° HEV rotation. At 0° rotation, although there is a notable increase in heat transfer efficiency, it is accompanied by a significant pressure drop, leading to higher pumping energy requirements, as seen in figs. 12 and 13.

At 15° rotation, on the other hand, there is a simultaneous improvement in both heat transfer efficiency and mixing index, resulting in a reduction in pressure drop. This suggests that the enhancement of mixing index plays a crucial role in mitigating pressure losses, thereby reducing the energy consumption associated with pumping. Analogous findings can be observed concerning the friction factor. Initially, at lower HEV rotation angles, higher friction factor values are recorded, indicating increased resistance to fluid flow. However, as the HEV rotation angle is augmented, a noticeable decrease in the friction factor is observed. This suggests that the introduction of HEV rotation plays a significant role in reducing the resistance to flow and mitigating pressure losses within the system.

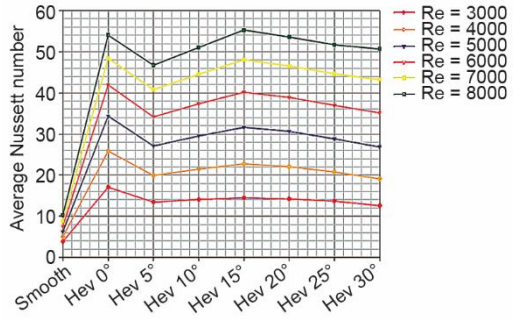

Figure 12. Average Nusselt number for different geometries

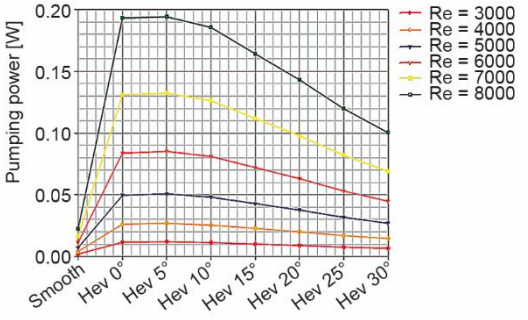

Figure 13. Pumping power for different geometries

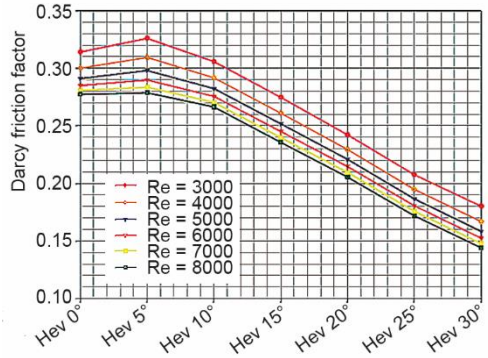

Figure 14. Darcy friction factor for different geometries

Furthermore, the effect of the Reynolds number on the friction factor must be considered. As the Reynolds number increased, it was observed that the friction factor exhibited a corresponding change. This behavior can be attributed to the dominance of inertial forces over viscous forces as the flow rate intensifies. As depicted in fig. 14, the friction factor exhibits a decreasing trend as Reynolds number increases, further accentuating the impact of fluid flow characteristics on the frictional losses experienced within the system.

Conclusions

Furthermore, the introduction of rotation in the HEV led to remarkable enhancements in both mixing index and heat transfer efficiency. As the rotation angle increased, the mixing index improved, resulting in a more homogeneous mixture of fluids. Simultaneously, there was a decrease in pressure drop, signifying reduced energy losses within the system. The rotational movement of the HEV proved to be a valuable factor in promoting efficient heat transfer and achieving an optimal balance between mixing performance and pressure drop.

Considering the combined effects of rotation, mixing index, pressure drop, and heat transfer, it is evident that a rotation angle between 15° and 20° in the HEV configuration yielded the most favorable outcomes. Within this range, an enhanced mixing index was achieved while maintaining an acceptable level of pressure loss. Furthermore, the introduction of rotation further improved the heat transfer efficiency, leading to more efficient thermal contact between the fluid streams.

References

[1] Valdes, J. P., *et al.*, Current Advances in Liquid–Liquid Mixing in Static Mixers: A Review, *Chemical Engineering Research and Design*, *177* (2022), Jan., pp. 694-731
[2] Jegatheeswaran, S., *et al.*, Laminar Mixing of Non-Newtonian Fluids in Static Mixers: Process Intensification Perspective, *Reviews in Chemical Engineering*, *36* (2022), 3, pp. 423-436
[3] Kaid, N., Ameur, H., Enhancement of the Performance of a Static Mixer by Combining the Converging/Diverging Tube Shapes and the Baffling Techniques, *International Journal of Chemical Reactor Engineering*, *18* (2020), 4, ID 20190190
[4] Meng, H., *et al.*, Experimental and Numerical Investigation of Turbulent Flow and Heat Transfer Characteristics in the Komax Static Mixer, *International Journal of Heat and Mass Transfer*, *194* (2022), Sept., ID 123006
[5] Hozumi, T., *et al.*, Nonlinear Pressure Drop Oscillations during Gelation in a Kenics Static Mixer, *Industrial & Engineering Chemistry Research*, *59* (2020), 10, pp. 4533-4541
[6] Hosseini, S. M., *et al.*, Design and Characterization of a Low-Pressure-Drop Static Mixer, *AIChE Journal*, *65* (2019) 3, pp. 1126-1133
[7] Karima, A., *et al.*, CFD Investigations of Thermal and Dynamic Behaviors in a Tubular Heat Exchanger with Butterfly Baffles, *Frontiers in Heat and Mass Transfer (FHMT)*, *10* (2018), Mar., 27
[8] Wongcharee, K., Eiamsa-Ard, S., Heat Transfer Enhancement by Twisted Tapes with Alternate-Axes and Triangular, Rectangular and Trapezoidal Wings, *Chemical Engineering and Processing: Process Intensification*, *50* (2011), 2, pp. 211-219
[9] Ghanem, A., *et al.*, Energy Efficiency in Process Industry – High-Efficiency Vortex (HEV) Multifunctional Heat Exchanger, *Renewable Energy*, *56* (2013), Aug., pp. 96-104
[10] Kaci, H. M., *et al.*, Effects of Embedded Streamwise Vorticity on Turbulent Mixing, *Chemical Engineering and Processing: Process Intensification*, *48* (2009), 10, pp. 1459-1476
[11] Liu, K., *et al.*, Design and Analysis of the Cross-Linked Dual Helical Micromixer for Rapid Mixing at low Reynolds Numbers, *Microfluidics and Nanofluidics*, *19* (2015), Feb., pp. 169-180
[12] Nanan, K., *et al.*, Heat Transfer Enhancement by Helically Twisted Tapes Inducing Co-and Counter-Swirl Flows, *International Communications in Heat and Mass Transfer*, *46* (2013), Aug., pp. 67-73
[13] Bahiraei, M., *et al.*, Development of Chaotic Advection in Laminar Flow of a Non-Newtonian Nanofluid: A Novel Application for Efficient Use of Energy, *Applied Thermal Engineering*, *124* (2017), Sept., pp. 1213-1223
[14] Habchi, C., *et al.*, Alternating Mixing Tabs in Multifunctional Heat Exchanger-Reactor, *Chemical Engineering and Processing: Process Intensification*, *49* (2010), 7, pp. 653-661
[15] Bakker, A., LaRoche, R. D., *Modeling of the Turbulent Flow in HEV Static Mixers*, The Online CFM Book at http://www.bakker.org/cfm
[16] Shi, H., *et al.*, Enhancing Heat Transfer of Drag-Reducing Surfactant Solution by an HEV Static Mixer with Low Pressure Drop, *Advances in Mechanical Engineering*, *3* (2011), ID 315943
[17] Promvonge, P., *et al.*, Heat Transfer in Square Duct Fitted Diagonally with Angle-Finned Tape, Part 1: Experimental Study, *International Communications in Heat and Mass Transfer*, *39* (2012) 5, pp. 617-624
[18] Promvonge, P., *et al.*, Heat Transfer in Square Duct Fitted Diagonally with Angle-Finned Tape, Part 2: Numerical study, *International Communications in Heat and Mass Transfer*, *39* (2012) 5, pp. 625-633
[19] Wang, L., *et al.*, Mixing Enhancement of a Passive Microfluidic Mixer Containing Triangle Baffles, *Asia-Pacific Journal of Chemical Engineering*, *9* (2014) 6, pp. 877-885
[20] Eissa, A., Simulation of the Turbulent Flow in HEV Static Mixers: Mixing of Ethanol With Gasoline, *Proceedings*, COMSOL Conference, Boston, Mass., USA, 2009
[21] Habchi, C., *et al.*, Intensifying the Turbulent Kinetic Energy Dissipation Rate by Redistributing Streamwise Vorticity, *Proceedings*, EPIC, European Process Intensification Conference, Venice, Italy, 2019
[22] Ameur, H., Effect of Corrugated Baffles on the Flow and Thermal Fields in a Channel Heat Exchanger, *Journal of Applied and Computational Mechanics*, *6* (2020) 2, pp. 209-218
[23] Boukhadia, K., *et al.*, Effect of the Perforation Design on the Fluid Flow and Heat Transfer Characteristics of a Plate Fin Heat Exchanger, *International Journal of Thermal Sciences*, *126* (2018), Apr., pp. 172-180

Paper submitted: October 10, 2022
Paper revised: March 26, 2023
Paper accepted: April 19, 2023